Sustainable Energy & Fuels

ROYAL SOCIETY OF CHEMISTRY

PAPER

View Article Online
View Journal | View Issue

Cite this: *Sustainable Energy Fuels*, 2023, **7**, 1974

Stable $FAPbI_3$ hydrate structure by kinetics negotiation for solar cells†

Ryan Taoran Wang, ‡[ab] Yu Zhang,‡[a] Xiaoxue Wu,[b] Weiwei Zhang,[c] Longxing Chi [c] and Fan Xu *[de]

Received 15th January 2023
Accepted 16th March 2023

DOI: 10.1039/d3se00062a

rsc.li/sustainable-energy

The instability of formamidinium lead iodide ($FAPbI_3$) perovskite has limited its application in renewable energy development, despite the highest power conversion efficiency (PCE) it exhibited. A step forward has been achieved here by negotiating the hydration kinetics *via* adjusting the moisture partial pressure. The stable hydrate was restricted to precipitating only in the area surrounding the grain boundary under the influence of the moisture partial pressure, avoiding the large strain created by the complete hydration reaction, which preserved the condensed morphology of the perovskite film. The PCE of such a device was thus enhanced to more than 10%, as opposed to the value of 0.32% in previous results, with comparable stability to the pure moisture-stable hydrate-based film, which not only provided a promising solution to the lifetime problem, but also provided fresh inspiration for thin film growth kinetics.

Introduction

Great progress has been achieved in perovskite solar cells (PSCs),[1,2] since the pioneering discovery of methylammonium lead iodide ($MAPbI_3$) in 2009.[3] The power conversion efficiency (PCE) of PSCs has increased from 3.9% to more than 25.7% with formamidinium lead iodide ($FAPbI_3$)-based devices, making them comparable to silicon cells.[4,5] The structure of $FAPbI_3$ has thus attracted a lot of attention recently, as it exhibited better stability and electrical conductivity[6–9] than the $MAPbI_3$ structure. These excellent properties enabled perovskite-related opto-electronic devices to be applied in many fields, such as space applications[10,11] and renewable energy development.[11–13] Unfortunately, the structure of $FAPbI_3$ experienced a phase transition at room temperature, which converted it from a cubic (α-phase) to hexagonal (δ-phase) structure, resulting in a rise in bandgap from ~1.5 eV to ~2.5 eV.[14–17] Even worse, the presence of water molecules could accelerate such a transition, which reduced the transition time from several hundred hours to only a few hours in a nitrogen gas atmosphere, causing a significant reduction in the PCE of the device.[18–20]

A large amount of research has been conducted to resolve this problem.[16,21–23] Some researchers have tried to replace some of the FA ions by smaller A-site cations, such as MA ions or caesium (Cs) ions.[24–26] They believed that the introduction of smaller ions in the A site could reduce the internal strain triggered by the oversized FA ions, which is the origin of the phase transition.[27] However, MA/Cs ions may segregate at the grain boundary during the operation, which is detrimental to device stability.[28,29] Others have tried surface passivation or encapsulation strategies.[30,31] For example, 2D perovskites were formed on top of the $FAPbI_3$ surface to passivate surface defects and increase the device lifetime.[18,32,33] However, the as-fabricated PSCs are still far from meeting the requirements of commercialization.

An important step forward has been achieved recently by Wang *et al.*[34] who discovered that $FAPbI_3$ could react with water moisture to generate the hydrate phase, filling the missing corner in the phase map of $FAPbI_3$ perovskite. A low-bandgap monohydrate phase was reported to be much more stable than the α-$FAPbI_3$ structure at room temperature, providing a scientific foundation for the solution to the challenge. Nevertheless, a device based on the monohydrate showed an efficiency of 0.32% despite the excellent stability, due to the generation of a large number of defects during the hydration reaction, which induced significant loss of photocurrent. Neither could surface healing be the solution, not only because of the large number of defects generated in the film, but also because of the impossibility of repairing the device during the operation.

It is therefore the purpose of the current research to resolve this problem by controlling the moisture partial pressure to investigate the hydration reaction kinetics. It has been revealed

[a]*College of Biophotonics, South China Normal University, 55 Zhongshan Ave W, Guangzhou, Guangdong, China, 510631*

[b]*Energy Materials and Optoelectronics Unit, Songshan Lake Materials Laboratory, China Academy of Sciences, Dongguan, Guangdong, China, 523808*

[c]*Department of Materials Science & Engineering, University of Toronto, 184 College St, Wallberg Memorial Building, Toronto, ON, Canada*

[d]*State Key Laboratory for Artificial Microstructure and Mesoscopic Physics, School of Physics, Frontiers Science Center for Nano-optoelectronics, Collaborative Innovation Center of Quantum Matter, Peking University, Beijing 100871, China. E-mail: xufan@pku.edu.cn*

[e]*Shenzhen BTR New Energy Technology Institute Co., Ltd, Shenzhen, Guangdong 518118, China*

† Electronic supplementary information (ESI) available. See DOI: https://doi.org/10.1039/d3se00062a

‡ These authors contributed to the work equally.

that the hydration reaction rate can be manipulated by the moisture partial pressure. In addition, at low partial pressure, water diffusion could also be suppressed. As a result, the hydrate phase will only be generated at the grain boundary area, which successfully passivates the film surface defects, not only effectively avoiding the creation of large internal strain by the complete hydration reaction, but also hindering water diffusion. The morphology of the original α phase was thus maintained, successfully preventing the PCE loss. Accordingly, the efficiency of hydrate-phase-based devices was increased by almost 60-fold, compared to our previous results,[34] taking a large step forward towards commercialization, which will hopefully be of interest to the broader research community in semiconductor thin films.

Experimental

Materials

All the commercial materials were used as received without further purification, including SnO_2 (15% in H_2O colloidal dispersion, Alfa Aesar), ethanol (AR Beijing Chemical Works), FAI (CH_5N_2I) (>99.98%, anhydrous Xi'an Polymer Light Technology Corp.), PbI_2 (99.999%, Sigma-Aldrich), chlorobenzene (99.9%, Sigma-Aldrich), isopropanol (IPA, 99.99%, Sigma-Aldrich), *N*,*N*-dimethylformamide (DMF, 99.99%, Sigma-Aldrich), dimethyl sulfoxide (DMSO, 99.9%, Sigma-Aldrich), Spiro-OMeTAD (Xi'an Polymer Light Technology Corp.), bis(-trifluoromethane)sulfonimide lithium salt (99.95%, Aldrich), 4-*tert*-butylpyridine (99.9%, Sigma-Aldrich), and ITO substrates.

Film and device fabrication

First, the ITO substrate was sequentially ultrasonicated twice with ethanol and acetone. The SnO_2 colloidal solutions (15 wt% in H_2O) were diluted with DI water to 2.67 wt%. After 30 min of UV-O_3 treatment, the diluted SnO_2 solutions were spin-coated at 3000 rpm for 30 s on ITO substrates, and then annealed on a hot plate at the displayed temperature of 150 °C for 30 min in ambient air. A two-step spin-coating method was adopted to prepare the perovskite layer. Specifically, 50 μL of PbI_2 solution were first spin-coated at 2000 rpm for 30 s and annealed at 70 °C for 1 min. Then, 100 μL of cation precursor solution were spin-coated at 1500 rpm for 30 s. The as-fabricated films were subsequently annealed at 150 °C for 30 min in air. Next, 50 μL of Spiro-OMeTAD solution doped with LiTFSI and tBP were spin-coated at 3000 rpm for 30 s. The hole transport material (HTM) solution was prepared by dissolving 60 mg of Spiro-OMeTAD, 30 μL of 4-*tert*-butylpyridine and 35 μL of Li-TFSI/acetonitrile (260 mg mL^{-1}) in 1 mL of chlorobenzene. Finally, 60 nm of Ag was thermally evaporated as a counter electrode under a pressure of 5×10^{-5} Pa on top of the hole transport layer to form the metal contact.

Characterization

X-ray powder diffraction (XRD) patterns were collected using a Bruker-AXS D8 DISCOVER X-ray diffractometer using CuKα1 radiation ($\lambda = 1.79026$ Å) in the range of 8°–78° (2θ) with a step size of 0.002° and a time setting of 0.1 s per step. Scanning electron microscopy (SEM) was carried out on a JEOL JSM-7000F instrument operating at a 0.1–5.0 kV landing voltage. The current density–voltage characteristics of the photovoltaic devices were obtained using a Keithley 2400 source-measurement system. The photocurrent was measured under AM 1.5G illumination at 100 mW cm^{-2} using a Newport Thermal Oriel 91192 1000 W solar simulator. The light intensity was calibrated using a KG-5 Si diode. The effective area of each cell was 0.102 cm^2, defined by masks for all the photovoltaic devices discussed in this work. Current density–voltage measurements were carried out at room temperature. A Nicolet 6700 FT-IR spectrometer was adopted for the FTIR measurements in the wavenumber range of 1000–3500 cm^{-1}, which has 0.09 cm^{-1} resolution with continuous dynamic alignment and an auto-tune function. UV-vis-NIR absorption spectroscopy was conducted with a Cary 5000 UV-vis-NIR spectrophotometer, from 800 nm to 300 nm. The photoluminescence measurements were conducted with a tunable Ar-ion laser from Melles Griot (35LAP431208) at a power of 130 mW with a repetition rate of 50 Hz. The time-resolved photoluminescence (TRPL) measurements were carried out on an FS5 fluorescence spectrometer at an excitation wavelength of 375 nm.

Results and discussion

In order to control the hydration reaction, the moisture partial pressure was reduced. Instead of adding water to the film directly, as has been done previously,[34] this time water vapor was injected into the perovskite film in the open environment. Fig. S1† schematically demonstrates these two processes. A fresh phenomenon was observed, as shown in Fig. 1a, where the lifetime of the α phase was increased to more than 7 days, as opposed to several hours of lifetime in the moist environment. The peak at 16.2° represents the (101) plane, which existed for more than 7 days in the controlled environment, indicating the presence of the α phase. In addition, the formation of the monohydrate phase was suppressed, as there is no peak present at 9° in Fig. 1a, while such a peak was generated after 12 hours in the closed humid chamber, as evidenced by Fig. 1b. The formation of dihydrate and trihydrate is also harder in this case, as can be proved by the relatively weak peaks at 13.7° and 23.5°, which represent the characteristic peaks for those phases. These results suggested that the formation of hydrate phases requires high moisture partial pressure/relative humidity (RH); otherwise, the water molecules tend to attack the perovskite film from an area of surface imperfection such as the grain boundary, resulting in a phase transition reaction only at such areas, which can be supported by previous modelling work.[8,35]

Such a discovery could also be evidenced by SEM measurements, which showed the morphological change of the α phase under the influence of moisture partial pressure. The pure α-phase thin film demonstrated small grain boundary areas and a large grain size of several hundred nanometers, as shown in Fig. 2a, which is consistent with previous related studies. After moisture treatment for 7 days in an open environment, little transition was observed in the film, as indicated in Fig. 2b, where the hydrate phase was only generated at the grain boundary area, from which the moisture diffusion began, leaving the bulk intact.

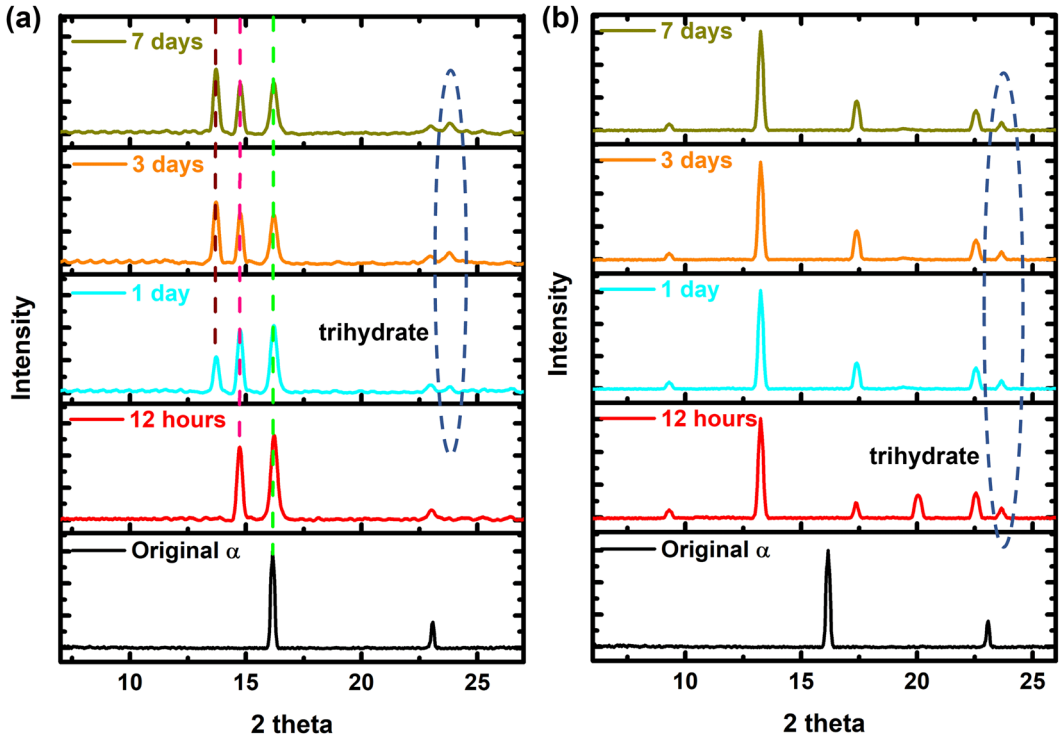

Fig. 1 (a) *In situ* XRD measurement of the perovskite film under reduced moisture partial pressure in an open environment. The peak at 16.2° represents the (101) plane of the α phase. The peak at 14.8° is the characteristic peak for the monohydrate phase. Peaks at 13.7° and 23.5° are generated by the dihydrate and trihydrate, respectively. Based on our previous research,[34] the monohydrate is the most stable phase in these hydrate phases, which means that, even if there is dihydrate or trihydrate, they will eventually convert to monohydrate. (b) *In situ* XRD measurement of the perovskite film after dropping water into the film, which showed a rapid hydration phase transition, as evidenced by the fast generation of the peaks at 13.7° and 23.5°.

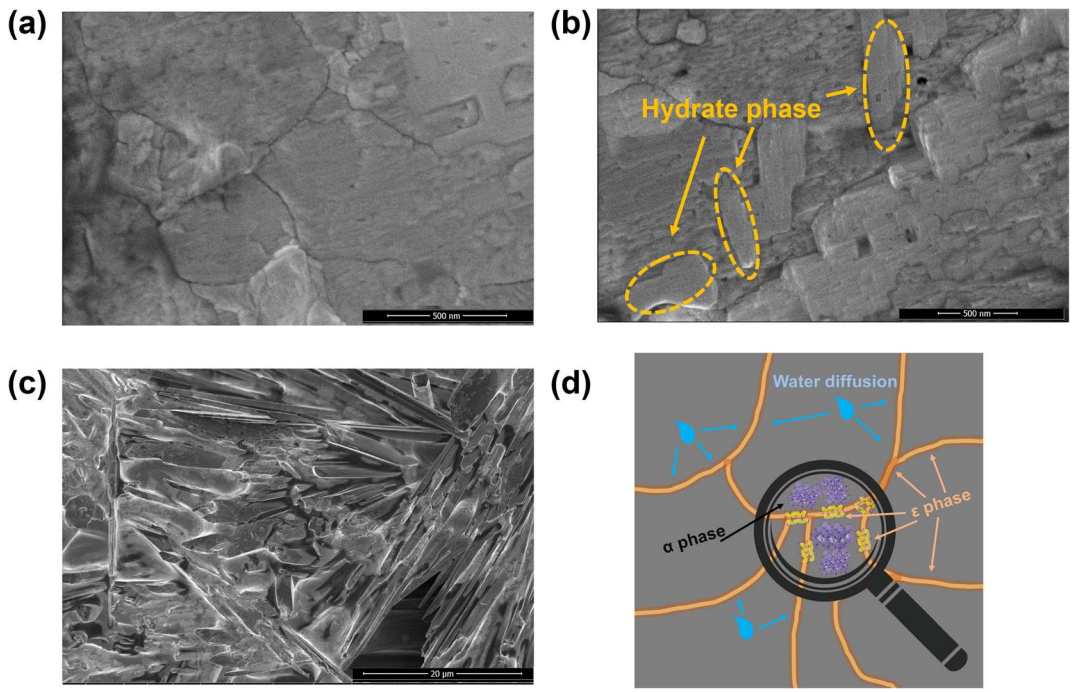

Fig. 2 (a) The SEM image of the film of pure α phase, which demonstrated a condensed morphology. (b) The SEM image of the film of moisture-treated perovskite, which has been exposed under reduced moisture partial pressure in an open environment for more than 7 days. Needle-shaped grains can be observed in the surroundings of the grain boundary. And there are some holes present, possibly due to the hydration reaction. (c) The SEM image of the fully hydrated perovskite film, which shows a large area of defects and needle-shaped grains, leading to great loss in PCE performance. (d) A schematic illustration of the diffusion and hydration reaction process under reduced water partial pressure. The hydrate phase could only be generated at the grain boundary area.

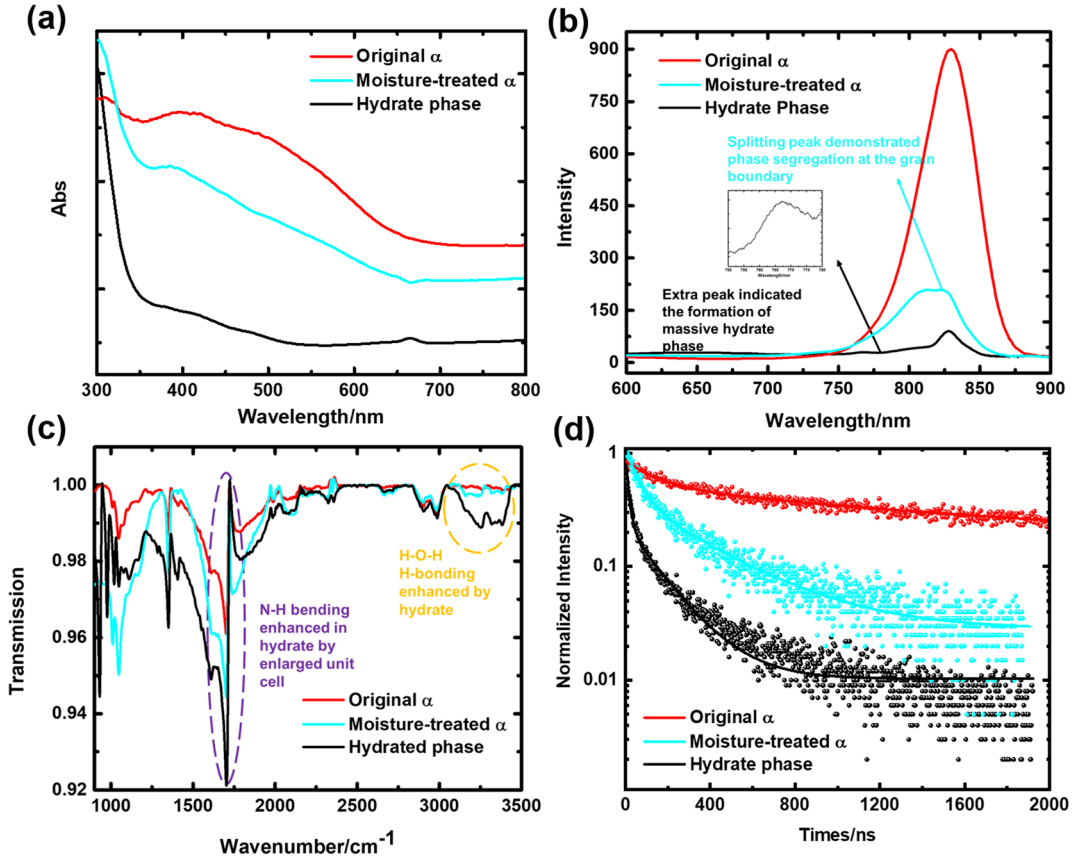

Fig. 3 (a) The UV-vis absorption spectroscopy of the various types of perovskite film. The α phase indicated a bandgap of around 1.55 eV. Both the moisture-treated and fully hydrated film showed a bandgap of around 1.77 eV. (b) The PL measurements of the various types of perovskite film, whose peak and half peak width demonstrate the carrier density in those films. (c) The FTIR spectroscopy measurements of the various types of perovskite film, which indicates the strengths and numbers of hydrogen bonds in those films. Raman spectroscopy has not been adopted as the perovskite structure is too sensitive to the excitation, which demonstrated strong peaks that overshadowed much other information.[36] (d) The TRPL measurements of the various types of perovskite film, which gave information about the carrier lifetime and indirectly reflected the defect areas in the perovskite films (more information is given in Table S1†).

A schematic diagram is also presented in Fig. 2d to illustrate the moisture diffusion and reaction at the perovskite thin film, which demonstrates how the condensed morphology is preserved by kinetic control over the hydration reaction. Such a morphology altered completely when the film was moisture treated in a closed chamber. Almost all the α phase was transformed into the hydrate phase, which demonstrated needle-shaped grains in the SEM image, as presented in Fig. 2c, resulting in a large number of defects, which is detrimental to the PCE performance. Even worse, such defects could hardly be repaired during the operation of the PSC device. Thus, it is necessary to control the hydration reaction of $FAPbI_3$ to maintain the beneficial morphology by reducing the moisture partial pressure, in which environment the hydrate phase only crystallizes in the grain boundary area, which will not only passivate the surface defects, but also stabilize the remaining α phase, effectively extending the lifetime of the device. It is now possible to negotiate the hydration kinetics to maintain both stability and PCE performance.

To verify these discoveries, we further examined the optical and chemical properties of the film, including UV-vis absorption, steady-state photoluminescence, Fourier-transform infrared spectroscopy (FTIR), and time-resolved photoluminescence (TRPL). As shown in Fig. 3a, the α phase exhibited an onset of absorption at around 800 nm by the extrapolation principle, which shifted to 800 nm after moisture treatment in the open environment, as opposed to absorption at 750 nm and 550 nm in the completely hydrated thin film. Such results were also indicated by the PL measurements, as demonstrated in Fig. 3b, where the curve of the original α phase showed much higher emission intensity, confirming the larger carrier density. In addition, more information can be extracted from the curves of the other two films. Split peaks were observed in the curve of the moisture-treated film, which demonstrated phase segregation at the grain boundary.[37,38] This means that the hydrate phase precipitated at the grain boundary instead of in the bulk, as has also been shown by the SEM results. The curve of the completely hydrated film, on the other hand, exhibited an extra peak at 760 nm (Fig. 3b inset), indicating the formation of the monohydrate inside the grain as a result of complete hydration, which could be further evidenced by the FTIR measurements. At 3000–3500 cm^{-1}, where the H–O–H vibration peaks are located, the absorption was greatly enhanced in the monohydrate thin

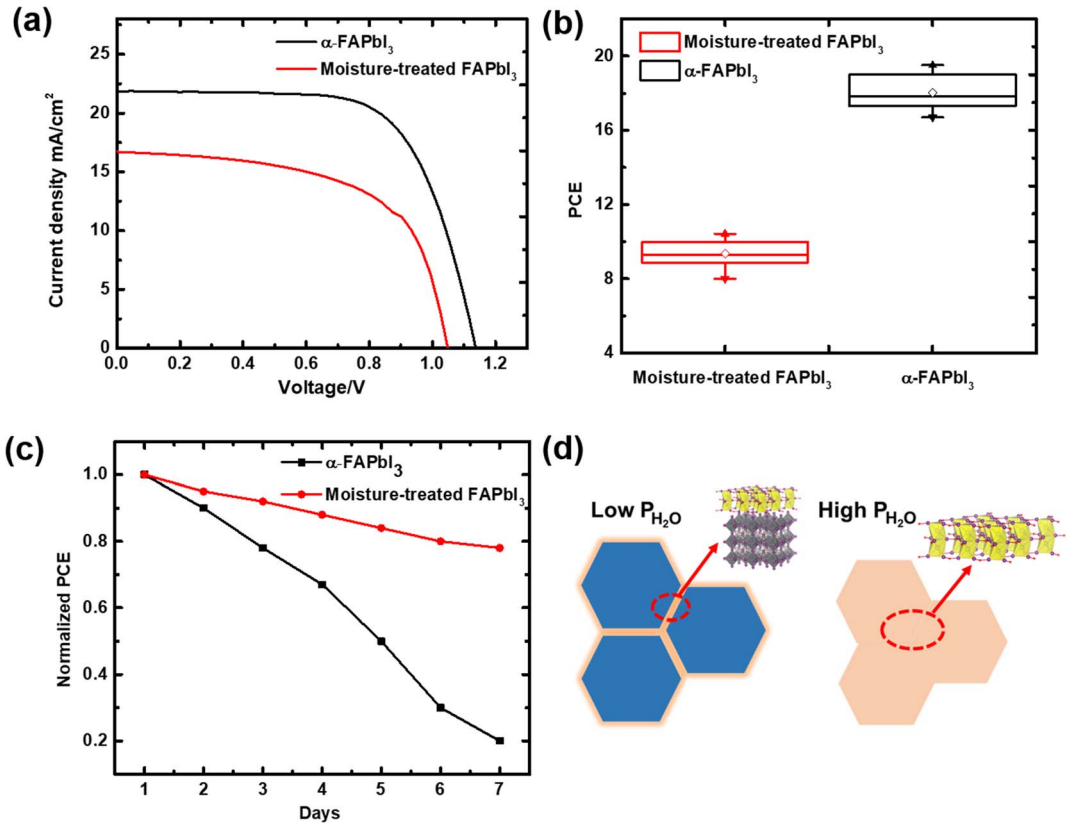

Fig. 4 (a) PCE measurements of the devices for the pure α phase and the moisture-treated α phase. Despite the efficiency losses, the PCE performance of the moisture-treated α phase is much better than that of the fully hydrated perovskite film, which showed a PCE of only 0.32%.[34] (b) Statistical PCEs of the pure α- and moisture-treated α-$FAPbI_3$ based PSCs. Each group contains twenty values for efficiency from different batches of cells. (c) The stability measurements of the devices for the pure α phase and the moisture-treated α phase under ambient conditions with RH of ~40%; the moisture-treated α phase showed a much longer lifetime. (d) A schematic illustration of the controlled hydration reaction by reduced moisture partial pressure.

film, as opposed to much less enhancement in the moisture-treated thin film, while the pure α-phase thin film showed little absorption in such a region, which indicated the number of hydrates in these films. As has been discovered before, the complete hydration transition would lead to the generation of massive internal strain, causing large amounts of defects in the film, which is why kinetic control has been adopted here to limit the formation of monohydrates. The TRPL results (Fig. 3d) further indicated less non-radiative recombination in the moisture-treated thin film than in the monohydrate-based film. The fitted TRPL data is summarized in Table S1.† Nevertheless, the original α-$FAPbI_3$ film showed an average carrier lifetime of 1500 ns, which is comparable to previous studies.[39] The moisture-treated perovskite film showed an enhanced lifetime of ~400 ns, which is better than that of the monohydrate-based film (~160 ns), indicating reduced non-radiative recombination and fewer defective areas.

In order to verify the beneficial effects of the controlled hydration reaction, current density–voltage measurements were conducted on both moisture-treated and control devices. The pure α-phase film was first synthesized and then moisture treated in an open environment to obtain the moisture-treated devices. All the PSCs adopted the device architecture of ITO/SnO_2/perovskite/Spiro-OMeTAD/Ag. Fig. 4a and b present the best *JV* curve and PCE distributions of the control and moisture-treated PSCs, respectively. The champion low partial pressure moisture-treated device exhibited a PCE of 10.4%, with the average PCE reaching 9.7% for the 20 devices, much better than the 0.32% of the fully hydrated perovskite film in our previous work.[34] The PSC stability measurements were conducted under ambient conditions with RH of ~40%. As shown in Fig. 4c, after 7 days of storage, the unencapsulated moisture-treated devices retained more than 80% of their original performance, while the control PSCs degraded by more than 80% in the same environment, due possibly to the presence of the hydrated phase, which is able to protect other layers, such as HTL, by absorbing water molecules. Compared to our previous pure-hydrate-based device,[34] the current low partial pressure moisture-treated device demonstrated comparable stability and much better PCE, which was enhanced by more than 18-fold. Clearly, such a change in the performance was caused by the moisture partial pressure, which demonstrated a great influence on hydrate growth. As shown in Fig. 4d, at lower moisture partial pressure, the water molecules could only diffuse into the grain boundary, generating the hydrate phase nearby, which passivated the film surface to protect the perovskite film. On the

other hand, at higher moisture partial pressure, the water diffuses rapidly into the grain, completely transforming the α-phase film, which created large amounts of defects, thereby reducing both film and device performance.

Summary

To summarize, the hydration kinetics between moisture and $FAPbI_3$ were investigated, which revealed the influence of moisture partial pressure on the formation of the hydrate phase. It has also been proved that the hydration reaction can be adapted to protect the $FAPbI_3$ film. The corresponding PSC devices exhibit similar stability to the fully hydrated devices generated at high moisture partial pressure, with an additional 30-fold enhancement in the PCE performance compared to the previous design,[34] attributed to negotiation of the hydration kinetics, which constrained the hydrate precipitation to only the grain boundary area, effectively passivating the film surface. The PCE of the low partial pressure moisture-treated device could be enhanced by more precise control over moisture diffusion, which is worthy of further investigation in a follow-up study. Hopefully, these discoveries could provide fresh guidelines for the novel design of PSC devices and inspire the broader research community to explore further the detailed physics involved.

Conflicts of interest

The authors declare no conflicts of interests.

Acknowledgements

This work was financially supported by the scientific projects of AECC Beijing Institute of Aeronautical Materials (202220941126A) and Guangdong overseas young talented postdoctoral support program. The authors would like to thank Prof. Gu Xu from McMaster University of Canada for his insightful discussion.

References

1 A. Mayer, T. Haeger, M. Runkel, J. Rond, J. Staabs, F. van gen Hassend, A. Röttger, P. Görrn, T. Riedl and H. C. Scheer, Relevance of Processing Parameters for Grain Growth of Metal Halide Perovskites with Nanoimprint, *Appl. Phys. A: Mater. Sci. Process.*, 2021, **127**(9), 717, DOI: **10.1007/s00339-021-04830-0**.

2 E. G. Tai, R. T. Wang, J. Y. Chen and G. Xu, A Water-Stable Organic-Inorganic Hybrid Perovskite for Solar Cells by Inorganic Passivation, *Crystals*, 2019, **9**(2), 83, DOI: **10.3390/cryst9020083**.

3 A. Kojima, K. Teshima, Y. Shirai and T. Miyasaka, Organometal Halide Perovskites as Visible-Light Sensitizers for Photovoltaic Cells, *J. Am. Chem. Soc.*, 2009, **131**(17), 6050–6051, DOI: **10.1021/ja809598r**.

4 S. Gharibzadeh, I. M. Hossain, P. Fassl, B. A. Nejand, T. Abzieher, M. Schultes, E. Ahlswede, P. Jackson, M. Powalla, S. Schäfer, M. Rienäcker, T. Wietler, R. Peibst, U. Lemmer, B. S. Richards and U. W. Paetzold, 2D/3D Heterostructure for Semitransparent Perovskite Solar Cells with Engineered Bandgap Enables Efficiencies Exceeding 25% in Four-Terminal Tandems with Silicon and CIGS, *Adv. Funct. Mater.*, 2020, **30**(19), 1909919, DOI: **10.1002/adfm.201909919**.

5 H. Zhou, J. Wang, M. Wang and S. Lin, Competing Dissolution Pathways and Ligand Passivation-Enhanced Interfacial Stability of Hybrid Perovskites with Liquid Water, *ACS Appl. Mater. Interfaces*, 2020, **12**(20), 23584–23594, DOI: **10.1021/acsami.0c03532**.

6 S. Masi, A. F. Gualdrón-Reyes and I. Mora-Seró, Stabilization of Black Perovskite Phase in $FAPbI_3$ and $CsPbI_3$, *ACS Energy Lett.*, 2020, 1974–1985, DOI: **10.1021/acsenergylett.0c00801**.

7 S. Akin, E. Akman and S. Sonmezoglu, $FAPbI_3$-Based Perovskite Solar Cells Employing Hexyl-Based Ionic Liquid with an Efficiency over 20% and Excellent Long-Term Stability, *Adv. Funct. Mater.*, 2020, **30**(28), 2002964, DOI: **10.1002/adfm.202002964**.

8 K. J. Xu, R. T. Wang, A. F. Xu, J. Y. Chen and G. Xu, Hysteresis and Instability Predicted in Moisture Degradation of Perovskite Solar Cells, *ACS Appl. Mater. Interfaces*, 2020, **12**(43), 48882–48889, DOI: **10.1021/acsami.0c17323**.

9 R. T. Wang, A. F. Xu, L. W. Yang, J. Y. Chen, A. Kitai and G. Xu, Magnetic-Field-Induced Energy Bandgap Reduction of Perovskite $KMnF_3$, *J. Mater. Chem. C*, 2020, **8**(12), 4164–4168, DOI: **10.1039/d0tc00088d**.

10 S. Song, S. J. Yang, W. Choi, H. Lee, W. Sung, C. Park and K. Cho, Molecular Engineering of Organic Spacer Cations for Efficient and Stable Formamidinium Perovskite Solar Cell, *Adv. Energy Mater.*, 2020, **10**(42), 2001759, DOI: **10.1002/aenm.202001759**.

11 R. K. Battula, G. Veerappan, P. Bhyrappa, C. Sudakar and E. Ramasamy, Stability of $MAPbI_3$ Perovskite Grown on Planar and Mesoporous Electron-Selective Contact by Inverse Temperature Crystallization, *RSC Adv.*, 2020, **10**(51), 30767–30775, DOI: **10.1039/d0ra05590e**.

12 A. Hassan, Z. Wang, Y. H. Ahn, M. Azam, A. A. Khan, U. Farooq, M. Zubair and Y. Cao, Recent Defect Passivation Drifts and Role of Additive Engineering in Perovskite Photovoltaics, *Nano Energy*, 2022, **101**, 107579, DOI: **10.1016/J.NANOEN.2022.107579**.

13 A. Abate, M. Saliba, D. J. Hollman, S. D. Stranks, K. Wojciechowski, R. Avolio, G. Grancini, A. Petrozza and H. J. Snaith, Supramolecular Halogen Bond Passivation of Organic-Inorganic Halide Perovskite Solar Cells, *Nano Lett.*, 2014, **14**(6), DOI: **10.1021/nl500627x**.

14 L. Qiu, S. He, Y. Jiang and Y. Qi, Metal Halide Perovskite Solar Cells by Modified Chemical Vapor Deposition, *J. Mater. Chem. A*, 2021, 22759–22780, DOI: **10.1039/d1ta06459b**.

15 M. R. Leyden, L. K. Ono, S. R. Raga, Y. Kato, S. Wang and Y. Qi, High Performance Perovskite Solar Cells by Hybrid Chemical Vapor Deposition, *J. Mater. Chem. A*, 2014, **2**(44), 18742–18745, DOI: **10.1039/c4ta04385e**.

16 S. Akin, E. Akman and S. Sonmezoglu, $FAPbI_3$-Based Perovskite Solar Cells Employing Hexyl-Based Ionic Liquid with an Efficiency over 20% and Excellent Long-Term

Stability, *Adv. Funct. Mater.*, 2020, **30**(28), 2002964, DOI: 10.1002/adfm.202002964.

17 A. F. Xu, R. T. Wang, L. W. Yang, E. E. Liu and G. Xu, An Environmentally Stable Organic–Inorganic Hybrid Perovskite Containing Py Cation with Low Trap-State Density, *Crystals*, 2020, 272, DOI: 10.3390/cryst10040272.

18 J. Wang, L. Liu, S. Chen, L. Qi, M. Zhao, C. Zhao, J. Tang, X. Cai, F. Lu and T. Jiu, Growth of 1D Nanorod Perovskite for Surface Passivation in $FAPbI_3$ Perovskite Solar Cells, *Small*, 2022, **18**(3), 2104100, DOI: 10.1002/smll.202104100.

19 M. Wang, Y. Yin, W. Cai, J. Liu, Y. Han, Y. Feng, Q. Dong, Y. Wang, J. Bian and Y. Shi, Synergetic Co-Modulation of Crystallization and Co-Passivation of Defects for $FAPbI_3$ Perovskite Solar Cells, *Adv. Funct. Mater.*, 2022, **32**(6), 2108567, DOI: 10.1002/adfm.202108567.

20 A. F. Xu, R. T. Wang, L. W. Yang, V. Jarvis, J. F. Britten and G. Xu, Pyrrolidinium Lead Iodide from Crystallography: A New Perovskite with Low Bandgap and Good Water Resistance, *Chem. Commun.*, 2019, **55**(22), 3251–3253, DOI: 10.1039/c8cc10135c.

21 R. T. Wang, A. F. Xu, J. Y. Chen, L. W. Yang, G. Xu, V. Jarvis and J. F. Britten, Reversing Organic-Inorganic Hybrid Perovskite Degradation in Water via PH and Hydrogen Bonds, *J. Phys. Chem. Lett.*, 2019, **10**(22), 7245–7250, DOI: 10.1021/acs.jpclett.9b02972.

22 C. Ma, B. Kim, D. H. Kang, S. W. Kim and N. G. Park, Nonchemical N- And p-Type Charge Transfer Doping of $FAPbI_3$ Perovskite, *ACS Energy Lett.*, 2021, **6**(8), 2817–2824, DOI: 10.1021/acsenergylett.1c01233.

23 M. Tan, B. Chen, Y. Zhang, M. Ni, W. Wang, H. Zhang, Q. Zhou, Y. Bao and Y. Wang, Temperature-Dependent Dynamic Carrier Process of $FAPbI_3$ Nanocrystals' Film, *J. Phys. Chem. C*, 2020, **124**(9), 5093–5098, DOI: 10.1021/acs.jpcc.0c01138.

24 O. A. Syzgantseva, M. Saliba, M. Grätzel and U. Rothlisberger, Stabilization of the Perovskite Phase of Formamidinium Lead Triiodide by Methylammonium, Cs, and/or Rb Doping, *J. Phys. Chem. Lett.*, 2017, **8**(6), 1191–1196, DOI: 10.1021/acs.jpclett.6b03014.

25 L. Xie, P. Song, L. Shen, J. Lu, K. Liu, K. Lin, W. Feng, C. Tian and Z. Wei, Revealing the Compositional Effect on the Intrinsic Long-Term Stability of Perovskite Solar Cells, *J. Mater. Chem. A*, 2020, **8**(16), 7653–7658, DOI: 10.1039/d0ta01668c.

26 H. Min, M. Kim, S. U. Lee, H. Kim, G. Kim, K. Choi, J. H. Lee and S. Seok, Efficient, Stable Solar Cells by Using Inherent Bandgap of a-Phase Formamidinium Lead Iodide, *Science*, 2019, **366**(6466), 749–753, DOI: 10.1126/science.aay7044.

27 G. Kim, H. Min, K. S. Lee, D. Y. Lee, S. M. Yoon and S. Seok, Impact of Strain Relaxation on Performance of A-Formamidinium Lead Iodide Perovskite Solar Cells, *Science*, 2020, **370**(6512), 108–112, DOI: 10.1126/science.abc4417.

28 G. Niu, H. Yu, J. Li, D. Wang and L. Wang, Controlled Orientation of Perovskite Films through Mixed Cations toward High Performance Perovskite Solar Cells, *Nano Energy*, 2016, **27**, 87–94, DOI: 10.1016/j.nanoen.2016.06.053.

29 P. Gratia, G. Grancini, J. N. Audinot, X. Jeanbourquin, E. Mosconi, I. Zimmermann, D. Dowsett, Y. Lee, M. Grätzel, F. de Angelis, K. Sivula, T. Wirtz and M. K. Nazeeruddin, Intrinsic Halide Segregation at Nanometer Scale Determines the High Efficiency of Mixed Cation/Mixed Halide Perovskite Solar Cells, *J. Am. Chem. Soc.*, 2016, **138**(49), 15821–15824, DOI: 10.1021/jacs.6b10049.

30 J. Suo, B. Yang, J. Jeong, T. Zhang, S. Olthof, F. Gao, M. Grätzel, G. Boschloo and A. Hagfeldt, Interfacial Engineering from Material to Solvent: A Mechanistic Understanding on Stabilizing α-Formamidinium Lead Triiodide Perovskite Photovoltaics, *Nano Energy*, 2022, **94**, 106924, DOI: 10.1016/j.nanoen.2022.106924.

31 Y. Zhou, J. Kwun, H. F. Garces, S. Pang and N. P. Padture, Observation of Phase-Retention Behavior of the $HC(NH_2)_2PbI_3$ Black Perovskite Polymorph upon Mesoporous TiO_2 Scaffolds, *Chem. Commun.*, 2016, **52**(45), 7273–7275, DOI: 10.1039/c6cc02086k.

32 Z. Zheng, S. Wang, Y. Hu, Y. Rong, A. Mei and H. Han, Development of Formamidinium Lead Iodide-Based Perovskite Solar Cells: Efficiency and Stability, *Chem. Sci.*, 2022, **13**(8), 2167–2183, DOI: 10.1039/d1sc04769h.

33 Y. Tang, Z. Gu, C. Fu, Q. Xiao, S. Zhang, Y. Zhang and Y. Song, $FAPbI_3$ Perovskite Solar Cells: From Film Morphology Regulation to Device Optimization, *Sol. RRL*, 2022, 2200120, DOI: 10.1002/solr.202200120.

34 R. T. Wang, A. F. Xu, W. Li, Y. Li and G. Xu, Moisture-Stable $FAPbI_3$ Perovskite Achieved by Atomic Structure Negotiation, *J. Phys. Chem. Lett.*, 2021, **12**(22), 5332–5338, DOI: 10.1021/acs.jpclett.1c01482.

35 A. F. Castro-Méndez, J. Hidalgo and J. P. Correa-Baena, The Role of Grain Boundaries in Perovskite Solar Cells, *Adv. Energy Mater.*, 2019, 1901489, DOI: 10.1002/aenm.201901489.

36 S. Ruan, D. P. McMeekin, R. Fan, N. A. S. Webster, H. Ebendorff-Heidepriem, Y. B. Cheng, J. Lu, Y. Ruan and C. R. McNeill, Raman Spectroscopy of Formamidinium-Based Lead Halide Perovskite Single Crystals, *J. Phys. Chem. C*, 2020, **124**(4), 2265–2272, DOI: 10.1021/acs.jpcc.9b08917.

37 H. Zhang, X. Fu, Y. Tang, H. Wang, C. Zhang, W. W. Yu, X. Wang, Y. Zhang and M. Xiao, Phase Segregation Due to Ion Migration in All-Inorganic Mixed-Halide Perovskite Nanocrystals, *Nat. Commun.*, 2019, **10**(1), 1088, DOI: 10.1038/s41467-019-09047-7.

38 S. G. Motti, J. B. Patel, R. D. J. Oliver, H. J. Snaith, M. B. Johnston and L. M. Herz, Phase Segregation in Mixed-Halide Perovskites Affects Charge-Carrier Dynamics While Preserving Mobility, *Nat. Commun.*, 2021, **12**(1), 6955, DOI: 10.1038/s41467-021-26930-4.

39 X. Chen, Y. Xia, Z. Zheng, X. Xiao, C. Ling, M. Xia, Y. Hu, A. Mei, R. Cheacharoen, Y. Rong and H. Han, In Situ Formation of δ-$FAPbI_3$ at the Perovskite/Carbon Interface for Enhanced Photovoltage of Printable Mesoscopic Perovskite Solar Cells, *Chem. Mater.*, 2022, **34**(2), 728–735, DOI: 10.1021/acs.chemmater.1c03505.

